







Article

Filter Cake Neural-Objective Data Modeling and Image Optimization

Dennis Delali Kwesi Wayo ^{1,2}, Sonny Irawan ^{1,*}, Alfredo Satyanaga ^{3,*}, Jong Kim ³,
Mohd Zulkifli Bin Mohamad Noor ² and Vamegh Rasouli ⁴

¹ Department of Petroleum Engineering, School of Mining and Geosciences, Nazarbayev University, Astana 010000, Kazakhstan; dennis.wayo@nu.edu.kz

² Faculty of Chemical and Process Engineering Technology, Universiti Malaysia Pahang Al-Sultan Abdullah, Kuantan 26300, Malaysia; mzulkifli@ump.edu.my

³ Department of Civil and Environmental Engineering, School of Engineering and Digital Sciences, Nazarbayev University, Astana 010000, Kazakhstan; jong.kim@nu.edu.kz

⁴ Energy and Petroleum Engineering Department, University of Wyoming, Laramie, WY 82071, USA; vrasouli@uwyo.edu

* Correspondence: irawan.sonny@nu.edu.kz (S.I.); alfredo.satyanaga@nu.edu.kz (A.S.);
Tel.: +7-77-1441-3590 (S.I.)

Abstract: Designing drilling mud rheology is a complex task, particularly when it comes to preventing filter cakes from obstructing formation pores and making sure they can be easily decomposed using breakers. Incorporating both multiphysics and data-driven numerical simulations into the design of mud rheology experiments creates an additional challenge due to their symmetrical integration. In this computational intelligence study, we introduced numerical validation techniques using 498 available datasets from mud rheology and images from filter cakes. The goal was to symmetrically predict flow, maximize filtration volume, monitor void spaces, and evaluate formation damage occurrences. A neural-objective and image optimization approach to drilling mud rheology automation was employed using an artificial neural network feedforward (ANN-FF) function, a non-ANN-FF function, an image processing tool, and an objective optimization tool. These methods utilized the Google TensorFlow Sequential API-DNN architecture, MATLAB-nftool, the MATLAB-image processing tool, and a single-objective optimization algorithm. However, the analysis emanating from the ANN-FF and non-ANN-FF (with neurons of 10, 12, and 18) indicated that, unlike non-ANN-FF, ANN-FF obtained the highest correlation coefficient of 0.96–0.99. Also, the analysis of SBM and OBM image processing revealed a total void area of 1790 M μm^2 and 1739 M μm^2 , respectively. Both SBM and OBM exhibited notable porosity and permeability that contributed to the enhancement of the flow index. Nonetheless, this study did reveal that the experimental-informed single objective analysis impeded the filtration volume; hence, it demonstrated potential formation damage. It is, therefore, consistent to note that automating flow predictions from mud rheology and filter cakes present an alternative intelligence method for non-programmers to optimize drilling productive time.

Keywords: mud rheology; filter cakes; neural network; image; objective optimization



Citation: Wayo, D.D.K.; Irawan, S.; Satyanaga, A.; Kim, J.; Bin Mohamad Noor, M.Z.; Rasouli, V. Filter Cake Neural-Objective Data Modeling and Image Optimization. *Symmetry* **2024**, *16*, 1072. <https://doi.org/10.3390/sym16081072>

Academic Editors: Laura Bulgariu and Alexander Zaslavski

Received: 23 January 2024

Revised: 21 March 2024

Accepted: 1 April 2024

Published: 19 August 2024



Copyright: © 2024 by the authors. Licensee MDPI, Basel, Switzerland. This article is an open access article distributed under the terms and conditions of the Creative Commons Attribution (CC BY) license (<https://creativecommons.org/licenses/by/4.0/>).

1. Introduction

An effective drilling mud formula is necessary to maintain smooth mud circulation in a wellbore. It ensures consistent hydrostatic pressure in the drilling column, the safe transport of cuttings, the efficient cooling of the drilling bit and string, and thorough hole cleaning [1]. These factors are critical in preventing fluid pressure from entering the wellbore and preventing blowouts [2,3]. However, the importance of proper mud engineering lies in the creation of mud cakes [4–7]. These cakes serve a dual purpose: they prevent the intrusion of formation fluids into the wellbore and also stop the filtration

of drilling fluids into the formation's pore throats, which could potentially damage the formation [8].

There have been numerous well-executed concepts for creating drilling fluids [9] that have been extensively studied as the most effective ways to prevent damage to a formation. Despite the abundance of available drilling fluid designs, the majority fall into two categories based on the materials used: oil-based and water-based. These commonly used muds have rheological profiles [10,11] that are highly responsive to the formation and are also environmentally friendly for both personnel and equipment. The rheological profiles [12,13] set by the American Petroleum Institute (API 13I) for these muds are specifically designed to optimize filtration and minimize damage near the wellbore while also improving drilling efficiency and reducing the non-productive time [14].

Fluids whose bases are synthetic have a long carbon chain history from C_{18} to C_{24} [15]. This organic compound is easily degradable but has extreme potency, behaving like an extract from crude oil as the base oils. However, this inverted emulsion has a continuous external phase, while the brine exhibits an internal phase. In addition, the popularity of synthetic fluids in markets today cannot be underestimated; ester, di-ether, poly-olefin, and detergent alkylate are examples. It is worth noting that some of these are formed by mixing alcohol with fatty acids, the condensation and oxidation of alcohols, the polymerization of ethylene, and alkylbenzene.

However, the presence of oil in synthetic-based muds [16] provides good hole cleaning and circulation, increasing the chance of protecting and persevering drilled formation walls. Moreover, this offers the advantage of providing no damageable traits to the drilling sections, which provides high performance in flat rheology. However, in shallow and deep wells [17] under drilling operations, some fluid engineers consider the efficiency of synthetic-based drilling fluids suitable fluids whose properties do not change over time or react inefficiently when in contact with high-temperature and high-pressure regions. Concerning aspects for which drilling is done in extremely cold regions, the flow behavior of the mud must maintain its physiochemical properties; these new formulations are experimented with and further researched to handle severe drilling conditions. Drilling fluids [18,19], and their hydraulics [20,21], are the basis for understanding computational flow geometry to handle efficient drilling operations.

Fluid hydraulics observe an API standard for measuring fluid rheology at the drilling site; mud engineers keep a close eye on the evaluation and monitoring of fluid properties to keep the well safe and balanced to prevent overwhelming situations [22]. The proficiency of the fluid in question is kept under rigorous tests for safe operations. These profiles under consideration take into account the density of the fluid, the apparent and plastic viscosity, the yield point, and gel strengths; the relevancy of this check helps ascertain the circulation and pressure loss of the drilling fluids' performances. Alsabaa [23] conducted a study on the flow properties of drilling mud, while Sedaghat and Kumar [24,25] examined mud rheology using the Marsh funnel and Fann 35 rotating viscometer, respectively. The continuous testing for the flat rheological properties of the synthetic-based drilling mud [26] in the fields and the laboratory remains a relevant job for rig crews to do because, when it comes to multilateral wells, suitable drilling fluids are designed to cater to well control. It is advisable to regularly assess the density of the fluid being used, particularly every 15–20 min, to identify any changes in its rheological properties. This frequent monitoring is necessary due to the potential interaction between the drilling fluids and sensitive formations.

While we tend to monitor and evaluate the drilling fluid profiles in a constant check, artificial and deep neural networks are greatly employed to reduce time–cost [27–29] effects on the drilling and production of hydrocarbons in the petroleum and civil engineering industries. Their application to solve complex and technical problems is derived from biological neuron concepts. This has the potential to solve linear and non-linear problems based on adaptable models and datasets. Moreover, optimizing the prediction of fluid rheology [30,31] requires an efficient computational model. The most reliable indicators for predicting the accuracy of machine learning outcomes are mean square errors (MSEs) and

the coefficient of correlation (R). A lower MSE value indicates a higher level of accuracy in the predictions, while a higher R-value (ranging from 0.7 to 0.9) signifies a stronger linear relationship between the variables.

As reported by Qamar [32], their previous research sheds light on optimizing gauge biofilm thickness and its hydrodynamic parameters using deep learning convolutional neural network algorithms. Their successful 2D and 3D biofilm thickness predictions were better than intuitive reasoning and manual calculations. Given this, the current study brings to light an intelligent means of predicting [33–36] the rheology of 498 sampled synthetic-based mud rheological profiles to determine and improve future drilling performance optimization expectations. The focus of this is to obtain or maximize filtration or the flow index for prediction and proper monitoring. In addition, the flow index computation from the neural network is a dependent variable of the entire fluid rheology parameters, recognizing PV, AV, and YP as its independent variables.

The accumulation of a thin layer of sludge on well walls is known as filter cake. Previous researchers [37–42] have developed methods to evaluate the effectiveness of drilling fluids under extreme pressure and temperature conditions. The ability of the cake to regain permeability or enhance hydrocarbon production after being washed away is explained due to the filtration loss. This study focused on laboratory-formulated synthetic-based [43] sludge, which allowed the liquid component of the sludge to seep into permeable formations, leaving behind compacted solid particles. These cakes with a higher thickness or tightly packed particles increase the drag and torque, making it easier for drilling pipes to get stuck during drilling. Conversely, when particles are loosely packed, it improves the porosity and permeability profiles, resulting in a favorable determination of the rheological profile.

There have been several widespread optimization algorithms to find optimal engineering design solutions. Based on the given problem or physics-informed objective functions, algorithms such as the Levenberg–Marquardt algorithm, gray wolf, ant colony, particle swarm optimization, the evolutionary algorithm, differential evolution, hill climbing, stochastic optimization, and now the most popular Adam algorithm [44] are widely used for optimization problems.

Also, the quest to find the flow index and maximize the filtration volume V_f for the optimum recovery of oil in filter cakes considers a physics-informed objective as described in the method section below, which focuses on the general single-objective optimization algorithm illustrated in the following Equations (1)–(4) [45]:

$$\min_x f(x) \text{ s.t.} \quad (1)$$

$$h_j(x) = 0; j = 1, \dots, m_e \quad (2)$$

$$g_j(x) = 0; j = 1, \dots, m_i \quad (3)$$

$$x_{\min} \leq x \leq x_{\max} \quad (4)$$

Dias and Liu [45,46] computed single- and multiple-objective optimizations for pultrusion and multistage filtration processes. Dias inferred informed physics and mathematics and then defined a pultrusion die with six heaters and C-section composite geometry.

While the current study optimized the filtration volume, V_f , based on a default genetic algorithm, Dias et al. [45] introduced two different algorithms for single-objective computation: particle swarm optimization (PSO) and sequential quadratic programming (SQP) algorithms. These algorithms were used under the influence of a constraint on the minimum degree of cure of 0.9. After drawing a comparative analysis, the sequential quadratic programming (SQP) algorithm performed better at 30.31% in determining the minimum objective function than that of particle swarm optimization (PSO).

Meanwhile, Liu computed a superstructure for the optimal design of a continuous, multistage reaction and crystallization process for the production of aspirin. The objective of the research problem was to maximize the yield and minimize waste under certain imposed constraints. The literature for this previous research sought to pay the maximum

attention to the wash filtration stage amongst other critical physics-informed components such as temperatures, the mass flow rate, and residence times. Despite several optimization scenarios, Liu maintained a genetic algorithm under single-objective computation to best define the optimal crystal size, yield, and coefficient of variation (CV). It, however, turned out that the respective mean crystal size and yield were 628 and 87.91, while the minimum coefficient of variation (CV) of 0.3596 was achieved.

The nature of pore spaces [47] and permeability capacity support fluid engineers' understanding of flow patterns and pore geometry through a permeable drilled formation. The current study supports the recognition and appreciation of the pore networks of solid particles [48] that are left behind due to synthetic-based mud after filtration. As the current study monitored the rheological profiles of the drilling fluid in operation, it is important that the crews on the rig site further visualize the flow geometry to recover oil. Rabbani and Jahari [49,50] studied the suspension of quantified solid particles and segments [51] for the flow patterns presented in 2D imagery; these techniques were informative to drilling management and to the current study. However, the data for testing, training, validation, image processing, and objective analysis [52–54] are discussed in the preceding sections.

The purpose of this study is to confirm the findings of previous experiments on mud rheology and filter cakes using hybrid artificial intelligent systems. The previous work lacked formal predictive analysis, so this study aims to fill that gap. Our motivation is to develop numerical modeling techniques that can be used by mud engineers without programming skills to monitor fluid rheology and filter cake formation using neural networks and computer vision.

2. Methodology

In this research framework, we demonstrated three different numerical methods to optimize the mud rheology parameters and fluid flow in filter cakes. Firstly, we organized laboratory data on mud rheology and integrated them into both the feed-forward neural network application and from Google TensorFlow open-source platform version 2.16.1. Secondly, we used MATLAB's image processing application to analyze the mud cake or filter cake image data generated during mud filtration. Finally, a genetic algorithm for a single-objective function based on the informed experiment was modeled. These techniques aided us in determining the amount of void spaces and predicting the permeability postures of the filter cakes and the flow index of the mud rheology. Here, as shown in Figure 1, we present a detailed discussion of the framework.

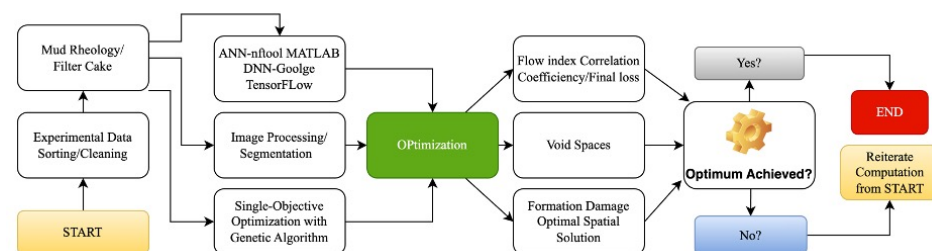


Figure 1. Computational framework for mud rheology flow predictions and filter cake image optimization.

2.1. Experimental Data

The rheology of synthetic-based mud was investigated in an experiment at Nazarbayer University's drilling fluid laboratory [55]. Data, as shown in Table 1, were collected and analyzed to understand the mud's rheological properties. To ensure accuracy, the data were sorted and filtered, removing any irrelevant information. A total of 498 data points were collected, including measurements of fluid density, viscosity, yield point, gel strength, and flow index.

Table 1. Statistical data for mud rheology.

	Density	R600	R300	PV	AV	YP	GS	FI
Mean	119.00	239.09	143.25	93.96	117.83	134.88	3.50	0.75
Std	0.83	24.74	24.94	2.02	11.89	1.41	0.50	0.10
Min	118.00	195.00	101.00	91.00	97.00	133.00	3.00	0.59
Median	119.00	240.00	143.00	94.00	118.00	135.00	3.00	0.75
Max	121.00	280.00	185.00	97.00	140.00	137.00	4.00	0.95

2.2. Neural Network Approach

Artificial neural networks, the most efficient and intelligent means of prediction [56,57], mimic the biological neural system as a means of reasoning to solve complex problems [58]. In recent years, the adoption of artificial neural networks (ANNs) has proliferated within the oil and gas industry, primarily to optimize various processes. Across the sector, a prevalent trend involves employing algorithms with three or more hidden layers within ANNs. The decision on the number of hidden layers hinges on the intricacy of the problems encountered and the richness of available data [59]. The input, hidden, and output layers were the only layers used in this study's data training, which supported the final model selection for an optimized prediction setting [60,61].

However, the relationship between layers is a deeply interconnected neuron network [62]. In this study, the artificial neural network feedforward function (ANN-FF) from MATLAB's nftool application, a user-friendly neural network processing toolbox meant for non-programmers, used the entire data from each fluid rheological component to model and predict better responses for fluid behavior [63,64]. The model was trained using inputs such as the plastic viscosity, apparent viscosity, yield point, and gel strength (10 s and 10 min) to determine the output flow index. This model is widely seen as effective because it can extract weights and biases from the trained data and the equations used. The already pre-processed data imported used 10, 12, and 18 neurons as a means to validate the results compared with Alsabaa's research [23]. Moreover, Figure 2a–l shows the propagation of more stable linear regression analysis by employing nftools' non-linear hidden neurons sigmoid with a linear output neuron based on the rheological parameters. While focusing on the computational speed with less memory accessibility, ANN-FF proceeded with the Levenberg–Marquardt training algorithm and the mean square error loss function.

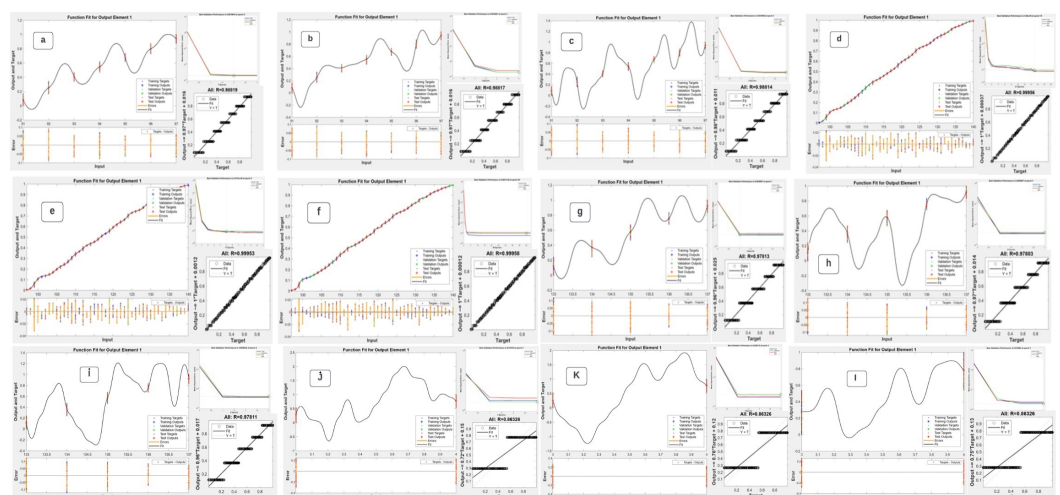


Figure 2. ANN-FF Correlation coefficient for respective 10, 12, and 18 hidden neurons; plastic viscosity: (a) = 0.98819, (b) = 0.98817, and (c) = 0.98814; apparent viscosity: (d) = 0.99956, (e) = 0.99953, and (f) = 0.99958; yield point: (g) = 0.97813, (h) = 0.97803, and (i) = 0.97811; and gel strength (10 min): (j) = 0.86326, (k) = 0.86326, and (l) = 0.86326.

Whereas ANN-FF was used to train 70%, validate 15%, and test 15% of the 498 datasets, the study further investigated the accuracy of a non-ANN-FF tool (OriginPro 2022 version 9.9.0.225) to validate the potency of the dataset in question, as demonstrated in Figure 3. However, the accuracy of this algorithm was achieved by monitoring the correlation coefficient R-value for each rheological property, as illustrated in Tables 2 and 3. The current study introduced the means to compute parameters for predictive analysis by maintaining Alsbaba's trained neurons for a fairer observation and validation process concerning how the network will coordinate the relationship between the input and output values to define accurate correlation coefficients.

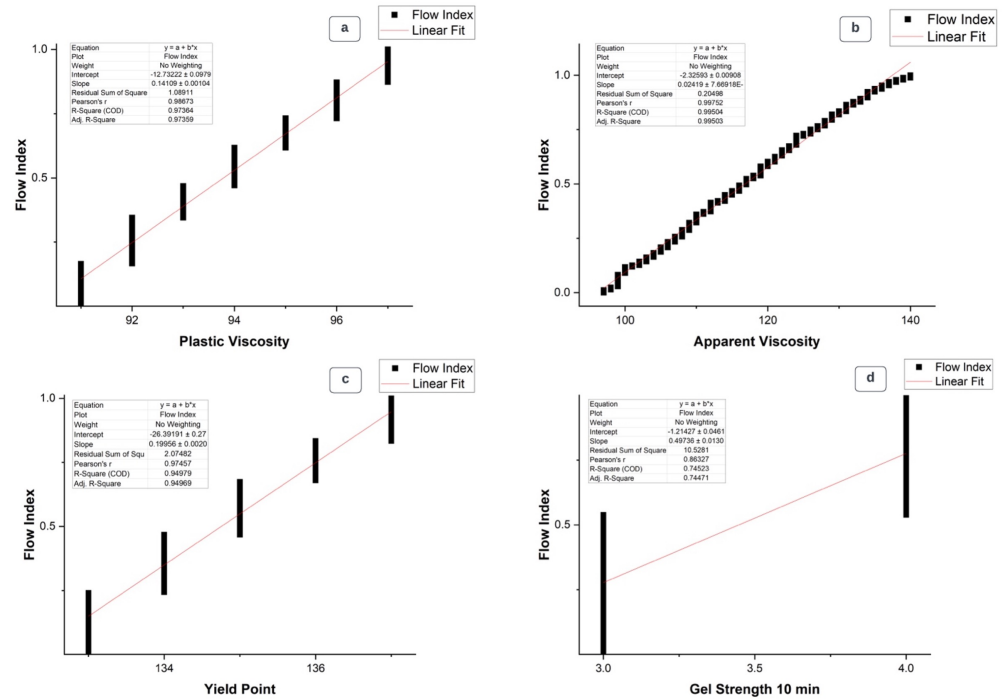


Figure 3. Non-ANN correlation coefficient: (a) PV, CC = 0.97359, (b) AV, CC = 0.99503, (c) YP, CC = 0.94969, and (d) GS 10 min, CC = 0.74471.

Table 2. ANN-FF rheological neuron analysis.

Property	Variable	Function	No. of Neurons	R	No. of Neurons	R	No. of Neurons	R
Plastic Viscosity	PV	FF	10	0.98819	12	0.98817	18	0.98814
Apparent Viscosity	AV	FF	10	0.99956	12	0.99953	18	0.99958
Yield Point	YP	FF	10	0.97813	12	0.97803	18	0.97811
Gel Strength (10 mins)	GS	FF	10	0.86326	12	0.86326	18	0.86326

Table 3. Rheological neuron and non-neuron model analysis.

Property	Variable	ANN-FF Model	Non-ANN-FF Model
		Average R	Adj. R ²
Plastic Viscosity	PV	0.98816	0.97359
Apparent Viscosity	AV	0.99956	0.99503
Yield Point	YP	0.97809	0.94969
Gel Strength (10mins)	GS	0.86326	0.74471

2.3. Filter Cake Image Processing

The interpretation of solid particles and their pore networks from the mud slurry was crucial for this study to support an easy visualization of flow geometry in order to better define the flow index. The images in Figure 4 are filter cakes from previous studies [55,65] that were captured and used for the interpretations. This process involved a MATLAB-Image Processing Toolbox; the embedded software is featured to recognize images and extract valid details in both quality and quantity. Data from these images were simply collated from their quantitative dimensional measurement and pixel segmentation; however, this analysis was based on color intensity, thus RGB and grayscale.

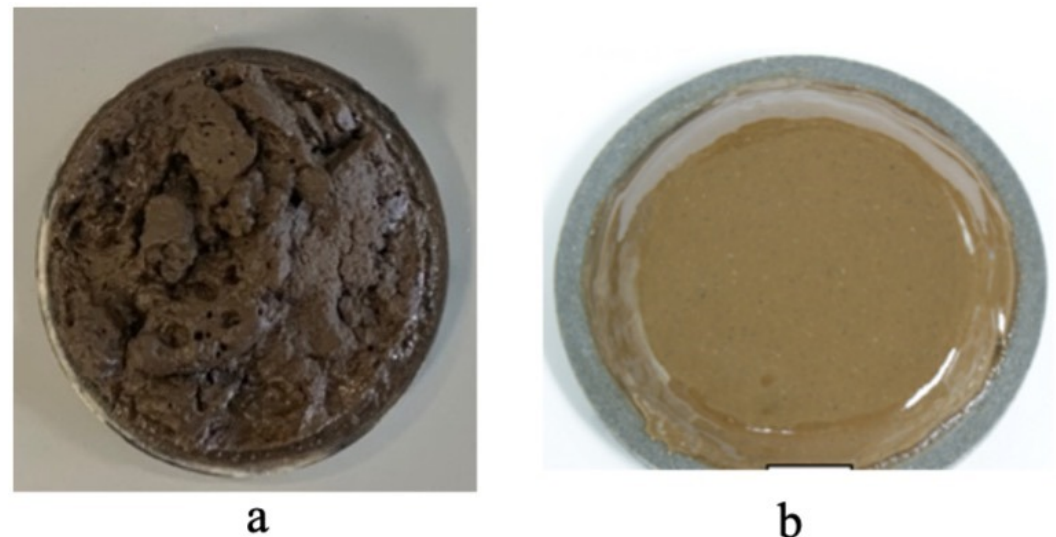


Figure 4. Images of laboratory filter cakes: (a) synthetic-based muds (b) oil-based muds.

The method simply has a simplified structured algorithm, as illustrated in Figure 5, where an input of the image gives rise to the output results; some techniques were employed while processing the image [66], and some of these are the region of interest (ROI), binary operations, the neighborhood and block, linear filtering and the filter, and a geometric operation, to mention but a few. While other previous studies [50] paid attention to binary image operations and regions of interest, the current study utilized the same, focusing on the entire mud cake as the region of interest and thresholding by converting full-color image or grayscale images into binary.

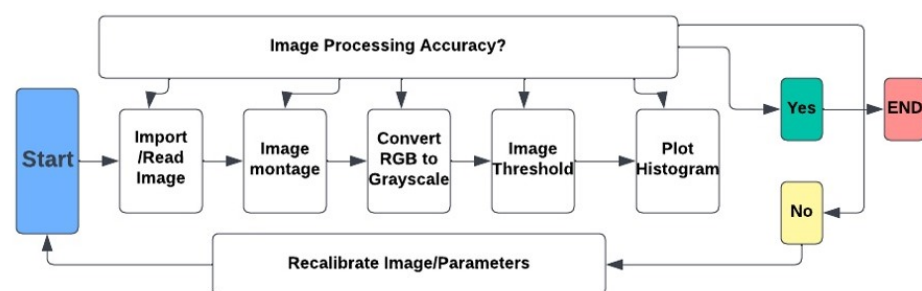


Figure 5. Flow chart for filter cake image processing.

Nevertheless, montage, an image editing technique, was used to effectively code the images from previous studies [55,65]; the analysis of these images converted them from their original colors (red, green, and blue—RGB) to grayscale and binary images [67,68]. As demonstrated in Figure 6, the intensity of the grayscale was rationed from 0 to 255; the lower the number, the darker it became, and the greater the number, the more grayscale

was attained. Also, the algorithm supports the conversion of grayscale to binary, and it is tuned according to its intensity from 0 to 1. The imported images [69,70] were partitioned into several visible fragments in a uniform pixel arrangement [71,72], and this process was seen as segmentation.

The next step after segmentation was thresholding, which involved the extraction of a partitioned image based on its intensity and properties. Further grayscale image interpretation for the current study fairly reviewed a 2D adjusted histogram of the two filter cakes, which were formulated from synthetic- and oil-based mud. The x–y axis of the histogram represents the respective intensities and amounts of pore spaces. A 3D particle distribution [73,74] and pore networks were initiated to explain how these two different mud compositions interact with permeability. Red, green, and blue (RGB) and hue saturation values (HSV) were selected for these processes. Thus, particle distribution [75] and particle suspension enhance simple visualization and expose the region of interest (ROIs); however, these processes are coined from thresholding.

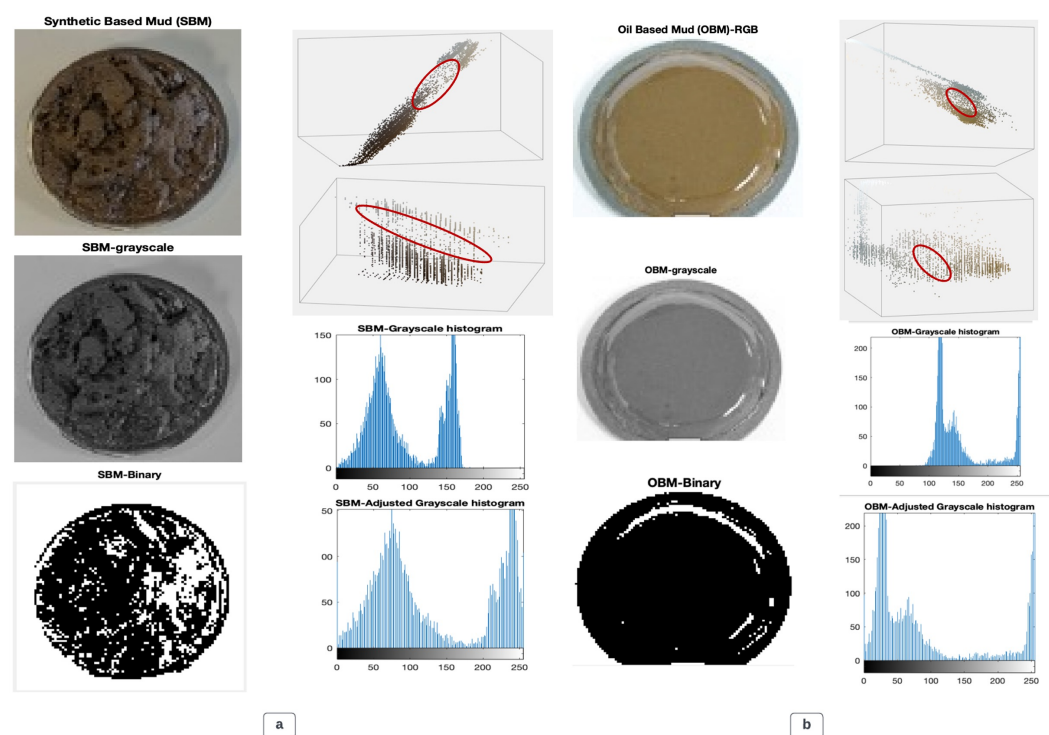


Figure 6. (a) Synthetic-basedmud filter cake image processing; PA: 1739 M μm^2 . (b) Oil-based mud filter cake image processing; PA: 1790 M μm^2 .

2.4. Flow Index Single-Objective Simulation

Through extensive optimization using a neural network and image processing, we achieved significant improvements in the flow index. We carefully derived an objective function and utilized a MATLAB optimization toolbox to process it. In Figure 7, we showcase the filtration flow in a ceramic disk, as simulated using a three-dimensional CFD simulation derived from the Oxford mathematical institute [76]. This simulation demonstrates the occurrence of flow in relation to the fluid and particle flow, the particle and pore sizes, and the irregular structures of ceramic pore throats.

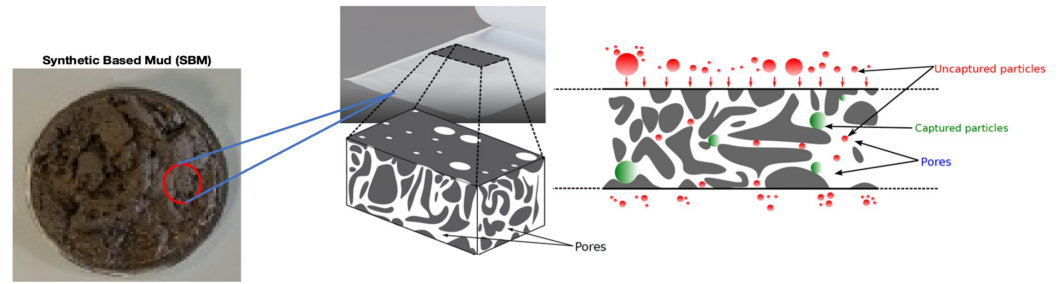


Figure 7. Schematic view of filter cake in CFD simulation adapted from Oxford mathematical institute website [76].

The single-objective simulation for the collated data presented a nitrogen gas injection in a carrier cell with a pressure of 20 psi for the recovery of oil through treated filter cakes on a ceramic disk. Optimizing or maximizing the flow index (filtration) in filter cakes for oil production would require narrowing the physics-based problem to a spatial solution. However, the study took inspiration from Puderbach's [77–80] filtration model, as presented in Equations (5) and (6), where R_m is the filter medium (ceramic disk), ΔP is the pressure drop, μ is the viscosity, A is the area, V_f is the filtration volume, r_k is the filter cake resistance, K_s is the filtration constant, and t is the filtration time.

$$\frac{t}{V_f} = \frac{\mu \cdot r_k \cdot K_s}{2 \cdot A^2 \cdot \Delta P} \cdot V_f + \frac{\mu}{A \cdot \Delta P} \cdot R_m \quad (5)$$

$$V_f = \frac{2 \cdot t \cdot A^3 \cdot \Delta P}{\mu \cdot A \cdot \Delta P (r_k \cdot k_s \cdot V_f + 2 \cdot A \cdot R_m)} \quad (6)$$

While satisfying the flow objective, the simulation considered holding other flow parameter constant, as indicated in Equation (7). However, maximizing the flow index would literally mean optimizing the filtration volume, V_f , and once the filtration volume were maximized, then the tendency of the treated filter cakes to produce or recover the required oil would have been achieved due to the porosity and permeability posture that the cake possesses.

$$f(x, y) = \frac{49.44 \cdot y}{42.81 \times x \cdot y + 0.0092} \quad (7)$$

Objective approximation:

$$f(x, y) = x^2 \cdot y^2 - 2 \cdot x \cdot y^2 + 3 \cdot y^2 \quad (8)$$

f(x,y) constraints for volume:

$$f(x, y) = 40 \text{ mL} \leq x \leq 200 \text{ mL} \quad (9)$$

f(x,y) constraints for pressure:

$$f(x, y) = 0 \text{ psi} \leq y \leq 35 \text{ psi} \quad (10)$$

The experimental data incorporated into this study expound on the analysis of several treated filter cakes undergoing oil-recoverable processes. This analysis demonstrated that, within 12 h of the initial oil recovery, the maximum filtration volume, V_f , was at 39.6 mL. However, the total 200 mL of synthetic oil recoverable was 200 mL, which indicated the following: the time that would be held constant in this objective would be 61 h for the complete oil recoverable process. This elaborates the model, as expressed in Equation (8); the filtration volume and pressure drop are replaced with the variables x and y , respectively. Whereas ' x ' represents the vertical nitrogen gas injection into the carrier cell, ' y ' illustrates the horizontal placement of the ceramic disk, coupled with the treated filter cakes and synthetic

oil in the carrier cell. As pressure was applied to the said carrier cell, oil was expected to flow through the treated filter cakes, whose polymeric strands were considered broken to optimize oil recovery processes. In simple terms, if oil takes a longer period to recover or to maximize the filtration volume in the graduated cylinder, then the ceramic disk would be considered damaged (formation damage) because the pore throats of the disk would be blocked due to several chemical impurities formed from improperly designed synthetic-based mud and treatment solutions.

3. Results and Discussion

3.1. Rheology Prediction Optimization

A predictive accuracy boost for the rheological parameters in this study required a high degree of a computational algorithm; this involved a sensitive analysis initiated via several neurons in the hidden layer used and the type of function the algorithm operated on. Though the study limited its data to 498 data points, the number of neurons increased significantly and had an impact on the correlation accuracy, as shown in Figure 8. This further explains the ineffectiveness of increasing the number of neurons since 10 and 12 neurons were enough to train and test the data. An increase in the number of neurons in this study yielded significantly low accuracy; however, the best number of neurons for the training for the said data was between 10 and 12.

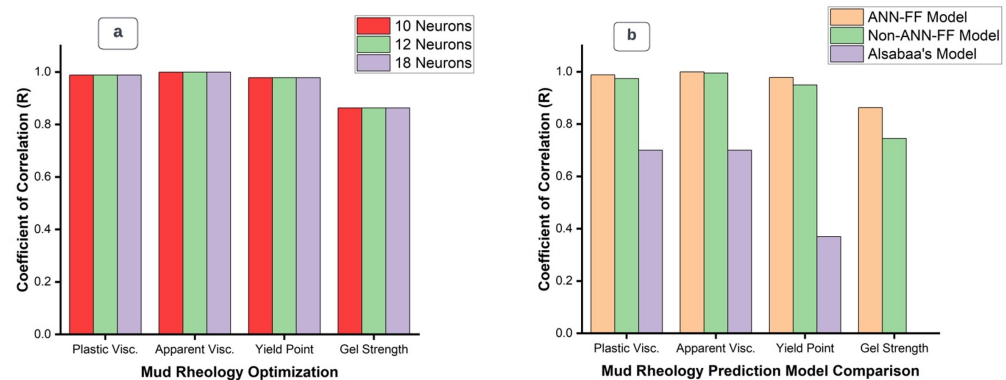


Figure 8. Flow index predictive analysis based on (a) neurons and (b) models.

The study further conducted a comparative analysis using Alsabaa's model and a non-ANN-FF linear fit model. The average of Alsabaa's mud weights' correlation coefficient (cc) and the average of the number of neurons is demonstrated in Figure 8b, which predicts the accuracy of the rheologically sensitive prediction analysis. The ANN-FF model from nftool clearly distinguishes between the best training and testing algorithms.

3.2. Cake Image Optimization

During image segmentation, an image-segmented app was loaded with an adjusted grayscale SBM image, and a high balanced threshold intensity of 90 was set for the SBM cake to attain a 2D binary image (black and white), as shown in Figure 6a. Morphology [81] at this stage was not necessary because there was no foreign interference in this analysis. Moreover, further segmentation was conducted to generate 3D particle image dispersion or image spacing, taking into account the SBM cake, and a color thresholding MATLAB app was launched. The SBM cake (actual color) was imported; scattered particle spacing is shown in Figure 6a, which includes the RGB and HSV. The region of concern is the visually dispersed particles indicating high porosity, which could also be simply identified using the less dense area of both the 3D scattered plot and the 2D binary image. It is worth noting that the study considered converting the actual pixels of the image to micrometers. The RGB-SBM image pixel area was 25,570, and the conversion to an area in micrometers yielded 1790 M μm^2 .

A similar segmentation algorithm for the oil-based mud (OBM) was applied; the image filter cake was imported and segmented using the embedded segmentation app, and the RGB image was converted into grayscale using the `im2gray` function and finally into a 2D binary image using the thresholding function. The threshold intensity of 90 used for the SBM was maintained for the OBM image processing; the color threshold exposed a 3D dispersity of particles in the OBM filter cake, as shown in Figure 6b. Notwithstanding, the entire area pixel of the filter cake was 24,846, whereas the micrometer area was 1739 M μm^2 . However, the analysis for this study focused on the 2D binary image and the 3D scattered particles; the binary image from Figure 6a,b explains, comparatively, that the SBM-binary had considerable amounts of white portions compared to the OBM-binary, which in effect means it had a greater tendency for increased permeability than the black portions, which tend to impede the flow [82]. Remarkably, the 3D scattered plots depict more flow accessibility for SBM than for OBM; this analysis was based on a standard thresholding intensity of 90 for both filter cakes to avoid computational biases and with the assumption that the cakes taken were of the same image quality. Figure 9 represents the area of void spaces in micrometers for SBM and OBM.

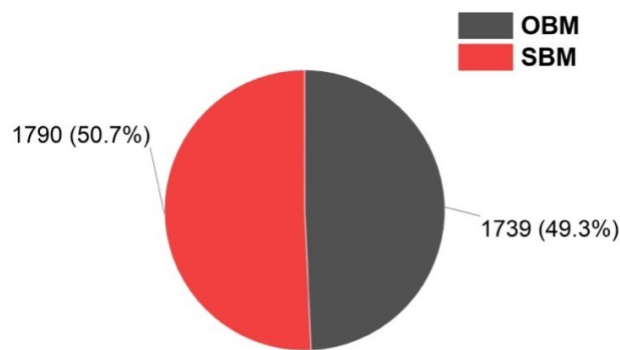


Figure 9. Comparative area of void spaces in synthetic-based and oil-based filter cakes.

3.3. Flow Index Single-Objective Optimization

The optimal solution with a genetic algorithm for this single extrapolated objective in Equation (8), based on Equations (5)–(7), resulted in $x = 0.6940$ and $y = 5.0536 \times 10^{-10}$. Though the computation was satisfactory at the optimum constraints given in Equations (9) and (10), the objective function was not feasible at a non-decreasing value. As indicated in Figure 10, the visual representation of the optimal solution demonstrated a possible fluid flow at the sharp edges of the graph, meaning that, while oil is possibly recoverable from formation damage, the edges of the ceramic disk would turn to give way to flow at a minimum induced pressure and a longer period. However, the analysis drawn indicates that the distribution of cake particles on the ceramic disk is quite uneven, thereby contributing to the solution of the extrapolated objective function.

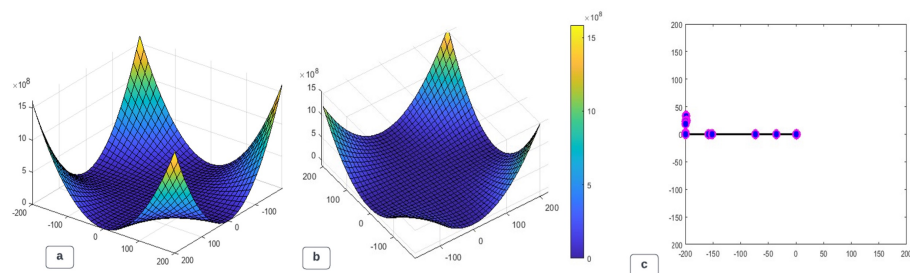


Figure 10. Three-dimensional single-objective modeling for filtration optimization: (a,b) optimal objective solution and (c) trace of the local maximum.

Algorithms from Google TensorFlow version 2.16.1. with emphasis on Keras architecture from Sequential APIs focused on importing the initial extrapolated objective with

the available experimental dataset to optimize the flow index. The object-based and other computed solutions were matched with the deep neural network optimal solution to satisfy the best model. Figure 11a,b show a scattered flow index response from its target in linear and non-linear regression with probability. The trained and tested data based on the extrapolated model and after several instances of tweaking indicated a final loss of 4.8, given that the trained models were optimized using the Adam optimizer at a learning rate of 0.01.

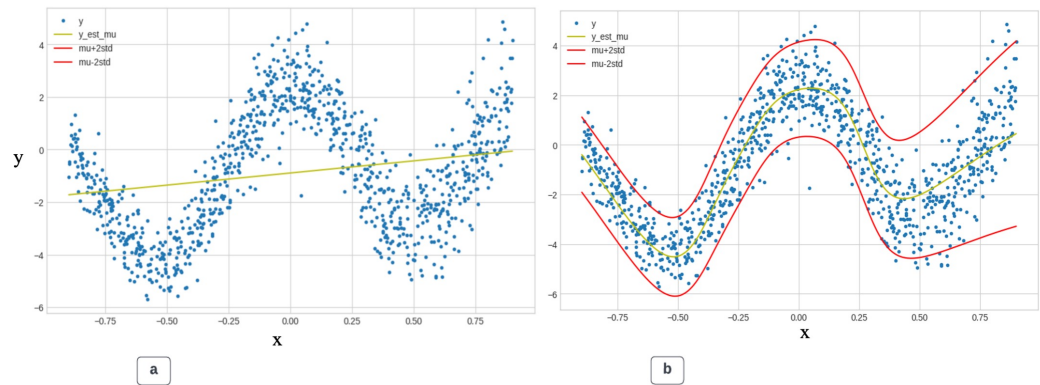


Figure 11. Neural-single-objective optimization: (a) linear and (b) non-linear.

The overall computational flow optimization analyses are shown in Table 3 to aid in the flow index optimization of the filter cake conclusions.

4. Conclusions

This study has introduced an automated method for computing rheological properties' high-frequency data that was specifically designed for individuals without programming experience. Utilizing the novel approach of neural-image-objective processing optimization, this technique predicts, monitors, and verifies the required algorithm. As a result, managers, operators, and engineers gain a deeper understanding of these tools, leading to more precise decision making. The following conclusions are derived from the computations, as demonstrated in Table 4.

Table 4. Neural-image-objective modeling analyses.

Model Architecture	Model Optimization
Artificial Neural Network (ANN-FF)	0.99956 cc
Non-Artificial Neural Network (Non-ANN-FF)	0.99503 cc
Image Processing (Synthetic-Based Muds)	1790 M μm^2
Single-Objective ($f(x, y) = x^2 \cdot y^2 - 2 \cdot x \cdot y^2 + 3 \cdot y^2$)	0.6940, 5.0536×10^{-10}
Deep Neural Network (DNN)–Final Loss	4.8

Neural Networks: By incorporating the feedforward function into the artificial neural network, the prediction of specific rheological properties was significantly improved. Specifically, when considering PV, AV, and YP, the accuracy reached an impressive 0.99 with 10 and 12 neurons. The non-ANN-FF model for rheological parameters exhibited an even better correlation efficiency of 0.99. The flow index, a property of particular interest for prediction, was focused on and iterated with 10, 12, and 18 neurons. This resulted in an accuracy of 0.97, making it an exceptional parameter compared to other neurons and models, as evidenced in Figure 8b. However, the automation of this number of neuron-driven flow indexes significantly contributed to effective predictive analysis. In addition to MATLAB's artificial neural network nftool, Google TensorFlow was employed to develop a deep neural network. The goal was to minimize the error function using the

Adam algorithm, which ultimately led to a final loss of 4.8. This achievement indicated the successful attainment of the flow index with the study's objective.

Image Processing: Separate investigations into oil- and synthetic-based mud filter cakes were conducted. Automating the visual pore structures of the two cakes indicated that the oil-based mud, with an area of $1739 \text{ M } \mu\text{m}^2$, had fewer pore spaces compared to the synthetic-based mud, whose area of pore spaces was $1790 \text{ M } \mu\text{m}^2$. There is an acceptable degree of erroneous image binary that emanates from the light intensity captured with the cameras in Figure 6a,b. The supposed area of void spaces could have been fairly eliminated or reduced if the images from the cameras used had a considerable amount of light intensity. Despite the pitfalls in processing, the image processing in a further probe revealed that the synthetic-based mud had an effective flow and good permeability. When using this constructive predictive analysis, the computational analysis conducted in this study with an image processing tool from MATLAB carefully reduces the time spent in the laboratory for designing effective mud.

Objective Optimization: The single-objective optimization for maximizing the filtration volume at this stage of the analysis validated the experimental data, in which longer periods (61 h) were achieved to recover oil from the treated filter cakes in the carrier cell. Despite objective approximations being far more considered and having impeded the flow at the center, the optimal solution for the simulation was at $x = 0.6940$ and $y = 5.0536 \times 10^{-10}$. The solution based on a genetic algorithm further concluded that the formation for recovering oil from the treated cakes was damaged. However, it also explains that the composition of the chemical solution for treatment might be at its minimum, and it suggests improving an eco-friendly filter cake wash. The quantities of nanoparticles for the formulation of the filter cake treatment solution could be minimized in grams to reduce the overlaying particles on the existing cake thickness.

In a nutshell, this research offers hybrid non-programming tools from MATLAB to define better fluid rheology and permeability predictions, which are easily accessible at the drilling site. Managers who are challenged with difficult predictive analysis and big data can use these non-programming tools to make and enforce the right decisions. However, further optimization for these findings could be extended for flow index predictions, computing CFD-DEM, and multiple-objective analysis, thereby making other exempted rheological parameters useful.

Author Contributions: Conceptualization, D.D.K.W. and S.I.; methodology, D.D.K.W.; validation, A.S., S.I. and J.K.; formal analysis, D.D.K.W. and S.I.; investigation, D.D.K.W., V.R. and M.Z.B.M.N.; resources, A.S., J.K. and S.I.; data curation, D.D.K.W.; writing—original draft preparation, D.D.K.W. and S.I.; writing—review and editing, V.R., S.I. and A.S.; visualization, D.D.K.W.; supervision, V.R., S.I., A.S. and M.Z.B.M.N.; project administration, A.S., J.K. and S.I.; funding acquisition, A.S., J.K. and S.I. All authors have read and agreed to the published version of the manuscript.

Funding: This research was funded by Nazarbayev University grant numbers 11022021CRP1512 and 08042FD1911, and the APC was funded by grant number 11022021CRP1512.

Data Availability Statement: The main data that support the findings of this study are openly available in the Nazarbayev University Repository at <http://nur.nu.edu.kz/handle/123456789/6132>, accessed on 22 June 2022, and the other data are duly referenced.

Acknowledgments: We are grateful to Nazarbayev University for providing us with the opportunity to continue sharing our work as part of the Collaborative Research Program (CRP) for the period of 2022–2024 with project number 11022021CRP1512. We again show our appreciation for the support of the Faculty-Development Competitive Research Grant for 2020–2022 (batch 2) with project number 08042FD1911. Additionally, we wholeheartedly thank the authors cited in this piece of writing for their extensive study that promotes knowledge sharing. Any opinions, findings, conclusions, or recommendations expressed in this material are those of the author(s) and do not necessarily reflect the views of Nazarbayev University.

Conflicts of Interest: The authors hereby declare that the research presented in this paper was not impacted by any known conflicting financial interests or personal connections.

Nomenclature

The following nomenclature is used in this manuscript:

2D	Two-dimensional
3D	Three-dimensional
ANN	Artificial neural network
APIs	Application programming interfaces
API	American Petroleum Institute
AV	Apparent viscosity
CFD	Computation fluid dynamic
CC	Coefficient correlation
CV	Coefficient of variation interfaces
DNN	Deep neural network
DEM	Discrete element method
FI	Flow index
FF	Feed-forward function
GA	Genetic algorithm
GS	Gel strength
HSV	Hue saturation value
MSE	Mean square error
OBM	Oil-based mud
PV	Plastic viscosity
PSO	Particle swarm optimization
R	Coefficient correlation
ROI	Region of interest
RGB	Red, green, and blue
RPM	Revolution per minute
R300	300-rpm shear stress
R600	600-rpm shear stress
SBM	Synthetic-based mud
SOO	Single objective optimization
SQP	Sequential quadratic programming
STD	Standard deviation
YP	Yield point
R_m	Filter medium
ΔP	Pressure drop, Pa
μ	Viscosity, cP
A	Area, m^2
V_f	Filtration volume, m^3
r_k	Filter cake resistance, m/kg
K_s	Filtration constant
t	Filtration time, s

References

- Skenderija, J.; Koulidis, A.; Sanchez, D.L.; Shehab, A. Advanced Hole Cleaning in Horizontal Wells: Experimental Investigation Supported by a Downhole Clamp-On Tool. In Proceedings of the Middle East Oil, Gas and Geosciences Show, Manama, Bahrain, 4–6 February 2023. [\[CrossRef\]](#)
- AlAwad, M.N.J. A new approach for understanding the mechanism of wellbore strengthening theory. *J. King Saud Uni. Eng. Sci.* **2022**, *34*, 67–76. [\[CrossRef\]](#)
- Kizayev, T.; Irawan, S.; Khan, J.A.; Khan, S.M.; Cai, B.; Zeb, N.; Wayo, D.D.K. Factors affecting drilling incidents: Prediction of suck pipe by XGBoost model. *Energy Rep.* **2023**, *9*, 270–279. [\[CrossRef\]](#)
- Salehi, S.; Ghalambor, A.; Saleh, F.K.; Jabbari, H.; Hussmann, S. Study of filtrate and mud cake characterization in HPHT: Implications for formation damage control. In Proceedings of the SPE European Formation Damage Conference and Exhibition, Budapest, Hungary, 3–5 June 2015. [\[CrossRef\]](#)
- Elkakatny, S. One-Stage Calcium Carbonate Oil-Based Filter Cake Removal Using a New Biodegradable Acid System. *Sustainability* **2019**, *11*, 5715. [\[CrossRef\]](#)
- Feng, Y.; Li, X.; Gray, K.E. Mudcake effects on wellbore stress and fracture initiation pressure and implications for wellbore strengthening. *Pet. Sci.* **2018**, *15*, 319–334. [\[CrossRef\]](#)

7. Amanullah, M.; Boyle, R. A Multifunctional Gel System to Mitigate Deepwater Drilling Challenges. In Proceedings of the International Oil & Gas Conference and Exhibition in China, Beijing, China, 8–10 December 2006; SPE-104080-MS. [CrossRef]
8. Galkin, V.I.; Martyushev, D.A.; Ponomareva, I.N.; Chernykh, I.A. Developing features of the near-bottomhole zones in productive formations at fields with high gas saturation of formation oil. *J. Min. Inst.* **2021**, *249*, 386–392. [CrossRef]
9. Aftab, A.; Ali, M.; Arif, M.; Chernykh, I.A. Influence of tailor-made TiO₂/API bentonite nanocomposite on drilling mud performance: Towards enhanced drilling operations. *App. Clay Sci.* **2020**, *199*, 105862. [CrossRef]
10. Liu, N.; Zhang, D.; Gao, H.; Hu, Y.; Duan, L. Real-time measurement of drilling fluid rheological properties: A review. *Sensors* **2021**, *21*, 3592. [CrossRef] [PubMed]
11. Husin, H.; Elraies, K.A.; Choi, H.J.; Aman, Z. Influence of graphene nanoplatelet and silver nanoparticle on the rheological properties of water-based mud. *App. Sci.* **2018**, *8*, 1386. [CrossRef]
12. Beg, M.; Kumar, P.; Choudhary, P.; Sharma, S. Effect of high temperature ageing on TiO₂ nanoparticles enhanced drilling fluids: A rheological and filtration study. *Upst. Oil Gas Tech.* **2020**, *5*, 100019. [CrossRef]
13. Murtaza, M.; Alarifi, S.A.; Kamal, M.S.; Onaizi, S.A.; Al-Ajmi, M.; Mahmoud, M. Experimental investigation of the rheological behavior of an oil-based drilling fluid with rheology modifier and oil wetter additives. *Molecules* **2021**, *26.1*, 4877. [CrossRef]
14. Candler, J.E.; Rushing, J.H.; Leuterman, A.J.J. Synthetic-based mud systems offer environmental benefits over traditional mud systems. In Proceedings of the SPE/EPA Exploration and Production Environmental Conference, San Antonio, TX, USA, 7–10 March 1993;. [CrossRef]
15. Growcock, F.B.; Andrews, S.L.; Frederick, T.P. Physicochemical properties of synthetic drilling fluids. In Proceedings of the IADC/SPE Drilling Conference, Dallas, TX, USA, 15–18 February 1994. [CrossRef]
16. Sayindla, S.; Lund, B.; Ytrehus, J.D.; Saasen, A. Hole-cleaning performance comparison of oil-based and water-based drilling fluids. *J. Petro. Sci. Eng.* **2017**, *159*, 49–57. [CrossRef]
17. Ay, A.; Dogan, H.A.; Sonmez, A. Drilling Fluids Project Engineering Guidance and Most Common Fluids Related Challenges for Deepwater and HPHT Offshore Wells. In Proceedings of the Offshore Technology Conference, Virtual and Houston, TX, USA, 16–19 August 2021. [CrossRef]
18. Fink, J. *Water-Based Chemicals and Technology for Drilling, Completion, and Workover Fluids*, 1st ed.; Gulf Prof. Pub.: Houston, TX, USA, 2015. [CrossRef]
19. Caenn, R.; Chillingar, G.V. Drilling fluids: State of the Art. *J. Petro. Sci. Eng.* **1996**, *14*, 221–230. [CrossRef]
20. Fadaïro, A.; Ling, K.; Rasouli, V.; Adelakun, A.; Tomomewo, O. An improved hydraulics model for aerated fluid underbalanced drilling in vertical wells. *Upst. Oil Gas Tech.* **2020**, *5*, 100009. [CrossRef]
21. Skenderija, J.; Koulidis, A.; Kelessidis, V.; Shehab, A. Application of a Drilling Simulator for Real-Time Drilling Hydraulics Training and Research. In Proceedings of the SPE Middle East Oil & Gas Show and Conference, Event Canceled, Sanabis, Bahrain, 28 November–1 December 2021. [CrossRef]
22. Martyushev, D.A.; Govindarajan, S.K. Development and study of a visco-elastic gel with controlled destruction times for killing oil wells. *J. King Saud Uni. Eng. Sci.* **2022**, *34*, 408–415. [CrossRef]
23. Alsabaa, A.; Gamal, H.; Elkattany, S.; Abdelraouf, Y. Machine Learning Model for Monitoring Rheological Properties of Synthetic Oil-Based Mud. *ACS Omega* **2022**, *7*, 15603–15614. [CrossRef] [PubMed]
24. Sedaghat, A.; Omar, M.A.A.; Damrah, S.; Gaith, M. Mathematical modelling of the Marsh Funnel for measuring rheological properties of drilling nanofluids for energy-efficient environment. In Proceedings of the International Conference on Ecological Vehicles and Renewable Energies (EVER), Monte Carlo, Monaco, 6–8 April 2016. Available online: <https://ieeexplore.ieee.org/abstract/document/7476401/authors> (accessed on 17 September 2023).
25. Kumar, V.; Guria, C. An improved shear rate estimation using rotating coaxial cylinder Fann viscometer. *J. Pet. Sci. Eng.* **2013**, *110*, 162–168. [CrossRef]
26. Oort, E.V.; Lee, J.; Friedheim, J.; Toups, B. New flat-rheology synthetic-based mud for improved deepwater drilling. In Proceedings of the SPE Annual Technical Conference and Exhibition, Houston, TX, USA, 26–29 September 2004. [CrossRef]
27. Lyros, E.; Kosteletzky, J.; Plicka, V.; Vratislav, F.; Sokos, E.; Nikolakopoulos, K. Detection of tectonic and crustal deformation using GNSS data processing: The case of ppnet. *Civ. Eng. J.* **2021**, *7*, 14–23. [CrossRef]
28. Goliatt, L.; Mohammad, R.S.; Abba, S.I.; Yaseen, Z.M. Development of hybrid computational data-intelligence model for flowing bottom-hole pressure of oil wells: New strategy for oil reservoir management and monitoring. *Fuel* **2023**, *350*, 128623. [CrossRef]
29. Silva, R.O.; Saporetti, C.M.; Abba, S.I.; Yaseen, Z.M.; Pereira, E.; Goliatt, L. An approach for total organic carbon prediction using convolutional neural networks optimized by differential evolution. *Neural Comp. App.* **2023**, *35*, 20803–20817. [CrossRef]
30. Balhoff, M.T.; Lake, L.W.; Bommer, P.M.; Lewis, R.E.; Weber, M.J.; Calderin, J.M. Rheological and yield stress measurements of non-Newtonian fluids using a Marsh Funnel. *J. Pet. Sci. Eng.* **2011**, *77*, 393–402. [CrossRef]
31. Sedaghat, A. A novel and robust model for determining rheological properties of Newtonian and non-Newtonian fluids in a marsh funnel. *J. Pet. Sci. Eng.* **2017**, *156*, 896–916. [CrossRef]
32. Qamar, A.; Kerdi, S.; Amin, N.; Zhang, X.; Vrouwenvelder, J.; Ghaffour, N. A deep neural networks framework for in-situ biofilm thickness detection and hydrodynamics tracing for filtration systems. *Sep. Purif. Technol.* **2022**, *301*, 121959. [CrossRef]
33. Elkattany, S. Real-time prediction of rheological parameters of KCL water-based drilling fluid using artificial neural networks. *Arab. J. Sci. Eng.* **2017**, *42*, 1655–1665. [CrossRef]

34. Elkatatny, S. Real-time prediction of the rheological properties of water-based drill-in fluid using artificial neural networks. *Sustainability* **2019**, *11*, 5008. [CrossRef]
35. Elkatatny, S. New approach to optimize the rate of penetration using artificial neural network. *Arab. J. Sci. Eng.* **2018**, *43*, 6297–6304. [CrossRef]
36. Souza, D.P.; Martinho, A.D.; Rocha, C.C.; Christo, E.D.S.; Goliatt, L. Hybrid particle swarm optimization and group method of data handling for short-term prediction of natural daily streamflows. *Model. Earth Syst. Environ.* **2022**, *8*, 5743–5759. [CrossRef]
37. Kabir, A.; Gamwo, I.K. Filter cake formation on the vertical well at high temperature and high pressure: Computational fluid dynamics modeling and simulations. *J. Pet. Gas Eng.* **2011**, *2*, 146–164. Available online: <https://api.semanticscholar.org/CorpusID:110719727> (accessed on 2 November 2023).
38. Falahati, N.; Chellappah, K.; Routh, A.F. Assessing filter cake strength via discrete element method simulations. *Chem. Eng. Res. Design* **2021**, *173*, 215–223. [CrossRef]
39. Elmgerbi, A.; Thonhauser, G.; Fine, A.; Hincapie, R.E.; Borovina, A. Experimental approach for assessing filter-cake removability derived from reservoir drill-in fluids. *J. Pet. Explor. Prod. Technol.* **2021**, *11*, 4029–4045. [CrossRef]
40. Aditama, P.; Mirza, M.; Iswachyono, T.; Anwar, Z.; Al Saadi, H.; Al Kalbani, M.; Qassabi, A.; Al Raqmi, M. Laboratory Testing Approach to Evaluate Drill-In-Fluid Damage and Wellbore Cleanup Effectivity in Open Hole Horizontal Producer Wells. In Proceedings of the SPE Asia Pacific Oil and Gas Conference and Exhibition, Jakarta, Indonesia, 22–24 October 2013. Abstract Number (SPE-166672-MS). [CrossRef]
41. Yang, M.; Li, M.; Wu, Q.; Growcock, F.B.; Chen, Y. Experimental study of the impact of filter cakes on the evaluation of LCMs for improved lost circulation preventive treatments. *J. Pet. Sci. Eng.* **2020**, *191*, 107152. [CrossRef]
42. Adebayo, A.R.; Bageri, B.S. A simple NMR methodology for evaluating filter cake properties and drilling fluid-induced formation damage. *J. Pet. Explor. Prod. Technol.* **2020**, *10*, 1643–1655. [CrossRef]
43. Israil, M.; Ashraf, M.; Fahim, M.; Rehan, R.; Khan, S.W.; Hussain, S. Evaluation of bentonite mixed indigenous clays for development of clay liners. *Civil Eng. J.* **2020**, *6*, 24–32. [CrossRef]
44. Wayo, D.D.K.; Irawan, S.; Satyanaga, A.; Kim, J. Data-Driven Fracture Morphology Prognosis from High Pressured Modified Proppants Based on Stochastic-Adam-RMSprop Optimizers; tf. NNR Study. *Big Data Cogn. Comp.* **2023**, *7*, 57. [CrossRef]
45. Dias, R.C.C.; Santos, L.S. Analysis of single and multi-objective optimization of the pultrusion process. *Mat. Today Com.* **2023**, *35*, 105677. [CrossRef]
46. Liu, J.; Benyahia, B. Single and Multi-Objective Superstructure Optimization of an Integrated Continuous Multistage Reaction-Crystallization-Filtration Process with Recycles. *Comp. Aided Chem. Eng.* **2023**, *52*, 667–672. [CrossRef]
47. Wu, S.; Zhu, W.; Chen, Y.; Liu, J.; Shu, S. Pore characteristics of cake and its effect on cake filtration. *Sep. Sci. Tech.* **2021**, *56*, 789–799. [CrossRef]
48. Kato, K.; Yamamoto, K.; Ogawa, N. Proposal for new image processing application for taste evaluation of sponge cake using 3D range sensor. *Sep. Sci. Tech.* **2008**, *56*, 63–67. [CrossRef]
49. Rabbani, A.; Ayatollahi, S.; Kharrat, R.; Dashti, N. Estimation of 3-D pore network coordination number of rocks from watershed segmentation of a single 2-D image. *Adv. Water Res.* **2016**, *94*, 264–277. [CrossRef]
50. Jahari, A.F.; Shafian, S.R.M.; Husin, H.; Razali, N.; Irawan, S. Quantification method of suspended solids in micromodel using image analysis. *J. Pet. Exp. Prod. Tech.* **2021**, *11*, 2271–2286. [CrossRef]
51. Habib, S.; Khan, I.; Aladhadh, S.; Islam, M.; Khan, S. External Features-Based Approach to Date Grading and Analysis with Image Processing. *Emerg. Sci. J.* **2022**, *6*, 694–704. [CrossRef]
52. Hernandez, M.; Quissak, F.; Córdova, M.; Torres, J. Synthetic Base Drilling Fluid Applications Under Extreme Pressure and Temperature Conditions in Gulf of Mexico. In Proceedings of the SPE Latin American and Caribbean Petroleum Engineering Conference, Virtual, 27–31 July 2020. [CrossRef]
53. Young, S.; Friedheim, J.; Lee, J.; Prebensen, O.I. A new generation of flat rheology invert drilling fluids. In Proceedings of the SPE Oil and Gas India Conference and Exhibition, Mumbai, India, 28–30 March 2012; Abstract Number (SPE-154682-MS). [CrossRef]
54. Herzhaft, B.; Peysson, Y.; Isambourg, P.; Delepouille, A.; Toure, A. Rheological properties of drilling muds in deep offshore conditions. In Proceedings of the SPE/IADC Drilling Conference, Amsterdam, The Netherlands, 27 February–1 March 2001; Abstract Number (SPE-67736-MS).
55. Primary Evaluation of Filter Cake Breaker in Biodegradable Synthetic-Based Drill-In-Fluid. Available online: <https://nur.nu.edu.kz/handle/123456789/6132> (accessed on 23 January 2024).
56. Wang, Y.; Salehi, S. Application of real-time field data to optimize drilling hydraulics using neural network approach. *J. Energy Res. Tech.* **2015**, *137*, 062903. [CrossRef]
57. Pitt, M.J. The Marsh funnel and drilling fluid viscosity: A new equation for field use. *SPE Dril. Comp.* **2000**, *15*, 3–6. [CrossRef]
58. Lippmann, R. An introduction to computing with neural nets. *IEEE ASSP Mag.* **1987**, *4*, 4–22. [CrossRef]
59. Elmgerbi, A.; Chuykov, E.; Thonhauser, G.; Andreas, N. Machine Learning Techniques Application for Real-Time Drilling Hydraulic Optimization. In Proceedings of the International Petroleum Technology Conference, Riyadh, Saudi Arabia, 21–23 February 2022. [CrossRef]
60. Agwu, O.E.; Akpabio, J.U.; Alabi, S.B.; Dosunmu, A. Artificial intelligence techniques and their applications in drilling fluid engineering: A review. *J. Pet. Sci. Eng.* **2018**, *167*, 300–315. [CrossRef]

61. Okrajni, S.S.; Azar, J.J. The effects of mud rheology on annular hole cleaning in directional wells. *SPE Drill. Eng.* **1986**, *1*, 297–308. [[CrossRef](#)]
62. Coussot, P.; Bertrand, F.; Herzhaft, B. Rheological behavior of drilling muds, characterization using MRI visualization. *Oil Gas Sci. Tech.* **2006**, *59*, 23–29. [[CrossRef](#)]
63. Maglione, R.; Robotti, G.; Romagnoli, R. In-situ rheological characterization of drilling mud. *SPE J.* **2000**, *5*, 377–386. [[CrossRef](#)]
64. Guria, C.; Kumar, R.; Mishra, P. Rheological analysis of drilling fluid using Marsh Funnel. *J. Pet. Sci. Eng.* **2013**, *105*, 62–69. [[CrossRef](#)]
65. Al-Ibrahim, H.; AlMubarak, T.; Almubarak, M.; Osode, P.; Bataweel, M.; Al-Yami, A. Chelating agent for uniform filter cake removal in horizontal and multilateral wells: Laboratory analysis and formation damage diagnosis. In Proceedings of the SPE Saudi Arabia Section Annual Technical Symposium and Exhibition, Al-Khobar, Saudi Arabia, 21–24 April 2015. [[CrossRef](#)]
66. Parmiggiani, F.; Moctezuma-Flores, M.; Wadhams, P.; Aulicino, G. Image processing for pancake ice detection and size distribution computation. *Int. J. Remote Sens.* **2019**, *40*, 3368–3383. [[CrossRef](#)]
67. Yang, W. Finite element model of concrete material based on CT image processing technology. *J. Vis. Com. Image Rep.* **2019**, *64*, 102631. [[CrossRef](#)]
68. Yu, F.; Sun, D.; Hu, M.; Wang, J. Study on the pores characteristics and permeability simulation of pervious concrete based on 2D/3D CT images. *Const. Build. Mat.* **2019**, *200*, 687–702. [[CrossRef](#)]
69. Xu, S.; Chang, C.; Liu, Y. A novel image compression technology based on vector quantisation and linear regression prediction. *Connect. Sci.* **2021**, *33*, 219–236. [[CrossRef](#)]
70. Yang, D.; Du, Y.; Yao, H.; Bao, L. Image semantic segmentation with hierarchical feature fusion based on deep neural network. *Connect. Sci.* **2022**, *34*, 1772–1784. [[CrossRef](#)]
71. Russell, B.C.; Torralba, A.; Murphy, K.P.; Freeman, W.T. LabelMe: A database and web-based tool for image annotation. *Int. J. Comput. Vis.* **2008**, *77*, 157–173. [[CrossRef](#)]
72. Xu, M.; Zhu, J.; Lv, P.; Zhou, B.; Tappen, M.F.; Ji, R. Learning-based shadow recognition and removal from monochromatic natural images. *IEEE Trans. Image Process.* **2017**, *26*, 5811–5824. [[CrossRef](#)] [[PubMed](#)]
73. Xu, M.; Li, M.; Xu, W.; Deng, Z.; Yang, Y.; Zhou, K. Interactive mechanism modeling from multi-view images. *ACM Trans. Graph.* **2016**, *35*, 236. [[CrossRef](#)]
74. Shen, X.; Maa, J.P. A camera and image processing system for floc size distributions of suspended particles. *Mar. Geo.* **2016**, *376*, 132–146. [[CrossRef](#)]
75. Wayo, D.D.K.; Irawan, S.; Khan, J.A.; Fitrianti. Validation for Assessing the Repercussions of Filter Cake Breakers; EDTA and SiO₂ on Filter Cake Return Permeability. *App. Art. Intel.* **2022**, *36*, 2112551. [[CrossRef](#)]
76. Oxford Mathematical Institute. Available online: <https://www.maths.ox.ac.uk/study-here/postgraduate-study/industrially-focused-mathematical-modelling-epsrc-cdt/infomm-resear-13/infomm-cohort-five/vey-mathematical-models-particle-filtration> (accessed on 17 March 2024).
77. Puderbach, V.; Schmidt, K.; Antonyuk, S. A coupled CFD-DEM model for resolved simulation of filter cake formation during solid-liquid separation. *Processes* **2021**, *9*, 826. [[CrossRef](#)]
78. Ripperger, S.; Gösele, W.; Alt, C.; Loewe, T. Filtration, 1. Fundamentals. *Ullmann's* **2013**, *14*, 678–709.
79. Junk, M.; Yong, W. Rigorous Navier-Stokes limit of the lattice Boltzmann equation. *Asymptot. Anal.* **2003**, *35*, 165–185. Available online: <https://content.iospress.com/articles/asymptotic-analysis/asy563> (accessed on 2 November 2023).
80. Stieß, M. *Mechanical Process Engineering—Particle Technology 1*, 3rd ed.; Springer: Berlin/Heidelberg, Germany, 2008; pp. XI, 499. [[CrossRef](#)]
81. Chu, C.P.; Lee, D.J.; Liu, Z.; Jin, W.H. Morphology of sludge cake at electroosmosis dewatering. *Sep. Sci. Tech.* **2005**, *39*, 1331–1346. [[CrossRef](#)]
82. Chase, G.G.; Willis, M.S. Flow resistance in filter cakes due to air. *Sep. Sci. Tech.* **1991**, *26*, 117–126. [[CrossRef](#)]

Disclaimer/Publisher's Note: The statements, opinions and data contained in all publications are solely those of the individual author(s) and contributor(s) and not of MDPI and/or the editor(s). MDPI and/or the editor(s) disclaim responsibility for any injury to people or property resulting from any ideas, methods, instructions or products referred to in the content.